PNAS RESEARCH ARTICLE | DEVELOPMENTAL BIOLOGY

Gonadal sex and temperature independently influence germ cell differentiation and meiotic progression in *Trachemys scripta*

Talia Hatkevich[a,1], Boris M. Tezak[a,b,1], Rafael D. Acemel[c,d], Vicky Wai Yee Chung[c], Dario G. Lupiáñez[c,d], and Blanche Capel[a,2]

Affiliations are included on p. 10.

Edited by R. Scott Hawley, Stowers Institute for Medical Research, Kansas City, MO; received July 5, 2024; accepted October 30, 2024

In species with genetic sex determination (GSD), the sex identity of the soma determines germ cell fate. For example, in mice, XY germ cells that enter an ovary differentiate as oogonia, whereas XX germ cells that enter a testis initiate differentiation as spermatogonia. However, numerous species lack a GSD system and instead display temperature-dependent sex determination (TSD). In the red-eared slider turtle, *Trachemys scripta*, a TSD model species with a warm female promoting temperature (FPT) and cool male promoting temperature (MPT) system, temperature directly affects germ cell number. In this study, we examined whether temperature directly affects other aspects of germ cell differentiation/sex identity. We uncoupled temperature and the sexual fate of the gonad by incubating eggs at MPT and treating with 17β-estradiol, a scheme that invariably produces ovaries. Through analysis of meiotic spreads, we showed that germ cells in FPT ovaries follow the typical pattern of initiating meiosis and progress through prophase I. However, in E2-induced ovaries that incubated at MPT, germ cells entered prophase I yet fail to exhibit synapsis. These results, combined with our single-cell transcriptome analysis, reveal a direct effect of temperature on germ cell sexual differentiation independent of its effect on the gonadal soma. These results imply that not all events of meiosis are under somatic control, at least not in this TSD species.

meiosis | sex determination | germ cell

Significance

In eutherian mammals, which exhibit XX/XY genetic sex determination (GSD), germ cell differentiation into oogonia or spermatogonia depends on whether an ovary or testis forms, which is controlled by XX or XY somatic cells. However, little is known about how germ cell sex identity is regulated in species in which sex is not determined genetically. We show that in a species with temperature-dependent sex determination (TSD), temperature directly affects germ cell sexual identity independent of the gonadal soma. We posit that meiotic progression in TSD species is dependent on the sexual identity of the somatic gonad, as well as a temperature cue that confers aspects of sexual identity on germ cells beginning prior to gonad differentiation.

Meiosis is a specialized type of cell division specific to germ cells of sexually reproducing organisms. The goal of meiosis in diploid organisms is to reduce the genome to produce haploid gametes. A hallmark of meiosis is the formation of cross-overs, which allows the reciprocal exchange of genetic information between the maternal and paternal homologs. Cross-overs also promote accurate segregation of the recombined homologous chromosomes at the end of meiosis I. To ensure cross-over formation between homologous chromosomes, the meiotic germ cell undergoes a tightly regulated series of events in prophase I of meiosis, involving characteristic chromosome dynamics for pairing, intentional DNA breakage, building of the synaptonemal complex, and the coordinated action of specialized DNA repair proteins. Studies in widely divergent taxa including *Caenorhabditis elegans, Saccharomyces cerevisiae*, *Drosophila melanogaster*, and *Mus musculus* have demonstrated that prophase I events are highly conserved (1).

Sex determination is the process by which an embryonic bipotential gonad, which contains undifferentiated somatic and germ cells, is directed toward testis or ovary differentiation through various signals. In organisms with genetic sex determination (GSD), gonadal differentiation signals are based on the presence or absence of dominant genetic determinants usually encoded on the sex chromosomes (2, 3). The relationship between meiotic entry and sex determination mechanisms has been elucidated for eutherian mammals, which exhibit XX/XY GSD. The sex chromosome genotype, XX or XY, directs the sexual differentiation of the somatic gonadal precursors into ovarian- (granulosa) or testis-specific (Sertoli) cell types (4). The resulting sexual identity of the gonadal soma in turn determines the sexual fate of the resident bipotential germ cells (5, 6). In this model, germ cells within an ovary enter meiosis embryonically, differentiating into a female, oogonial fate. Alternatively, germ cells surrounded by a testicular soma enter a G0 mitotic arrest, thereby committing to a male, spermatogonial fate (7, 8).

In other taxa, including some fish and reptiles, genes do not have a strong influence on sex determination. Instead, several species from these taxa can use temperature to determine their phenotypic sex (temperature-dependent sex determination, TSD) (9) (Fig. 1*A*). In TSD species, the gonadal sex of an individual is sensitive to temperature cues experienced during a critical period of embryonic development, termed the thermosensitive period (TSP). In contrast to mammals, in which the genetic determinant of sex is expressed and acts in a specific cell type (the somatic cells within the developing gonad), there is no a priori

Author contributions: T.H., B.M.T., and B.C. designed research; T.H., B.M.T., R.D.A., and V.W.Y.C. performed research; T.H., B.M.T., R.D.A., and D.G.L. analyzed data; and T.H., B.M.T., R.D.A., D.G.L., and B.C. wrote the paper.

The authors declare no competing interest.

This article is a PNAS Direct Submission.

[1]T.H. and B.M.T. contributed equally to this work.

[2]To whom correspondence may be addressed. Email: blanche.capel@duke.edu.

This article contains supporting information online at https://www.pnas.org/lookup/suppl/doi:10.1073/pnas.2413191121/-/DCSupplemental.

Published December 30, 2024.

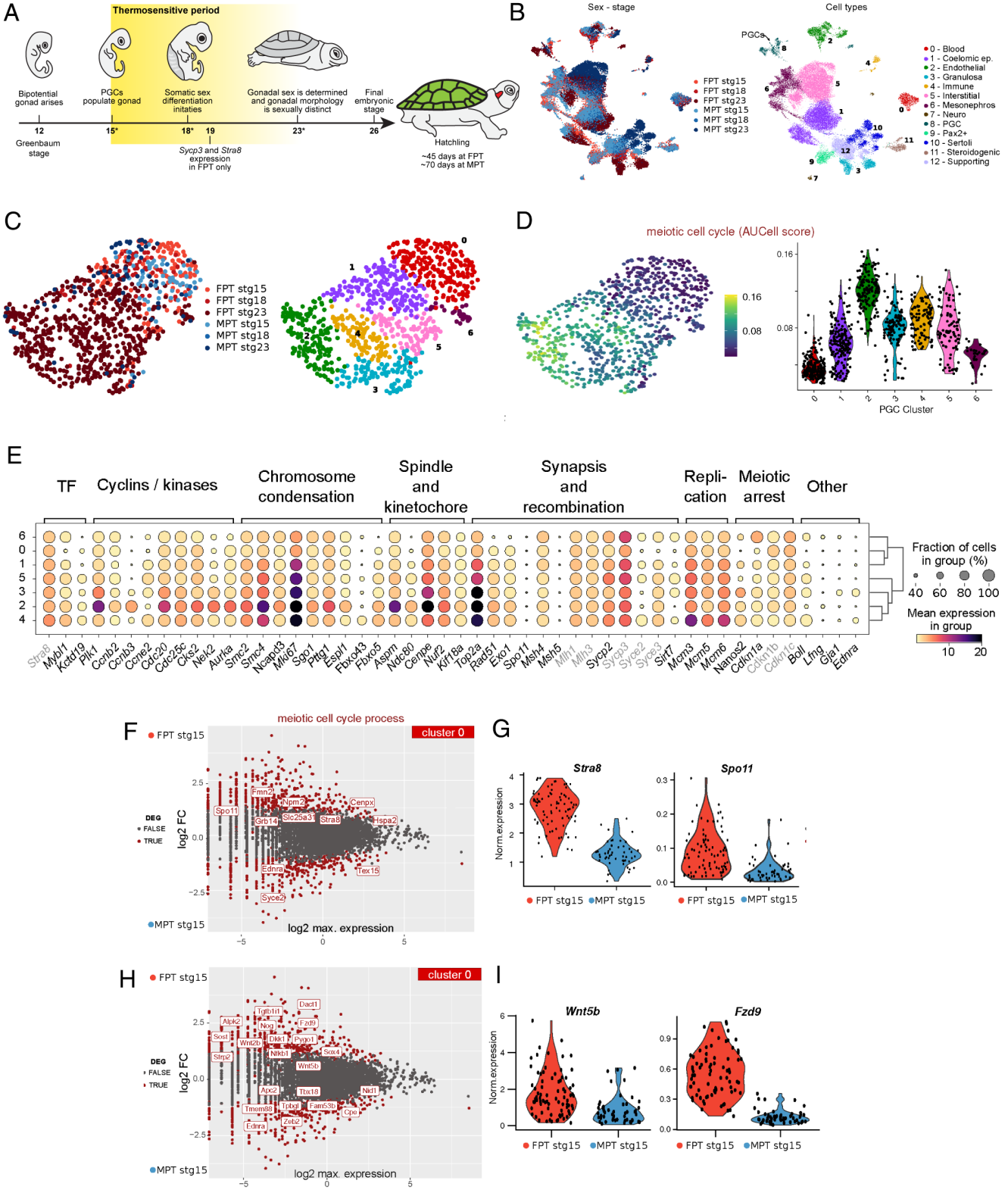

Fig. 1. Single-cell transcriptomics reveal heterogeneous meiotic gene expression throughout the TSP. (*A*) Events of gonadal development in *T. scripta*. Asterisks indicate stages analyzed for single-cell transcriptomics. (*B*) *Left*: SCVI-integrated UMAP of *T. scripta* gonads during somatic sex determination with colors representing the sample of origin (FPT = Female producing temperature, MPT = Male producing temperature). *Right*: Same UMAP as in A but colored according to cell types. (*C*) *Left*: SCVI-integrated UMAP of germ cells. *Right*: UPMAP colored according to the subclustering. (*D*) UMAP colored with the AUCell score of genes belonging to the GO term meiotic cell cycle (*Left*). *Right*: Violin plot of the same AUCell scores split by subclusters. (*E*) Dot plot of differentially expressed genes in the different clusters. Colors represent the mean expression in the clusters and the size of the dots the proportion of cells in the cluster where the transcript is detected. Additional genes related to meiosis but not found to be differentially expressed among clusters were also added (written in gray). (*F*) MA plots showing differentially expressed genes within subcluster 0 between FPT and MPT cells. Meiotic cell cycle process genes are indicated. (*G*) Violin plot with the expression of two representative meiotic cell cycle process genes. (*H*) MA plots showing differentially expressed genes within subcluster 0 between FPT and MPT cells for the WNT signaling pathway. (*I*) Violin plot with the expression of *Wnt5b* and *Fzd9*.

reason why the effects of temperature on sex determination should be limited to a single cell lineage. This led us to question whether the fate of germ cells is controlled by the gonadal soma in TSD species or whether it is independently influenced by temperature.

The red-eared slider turtle, *Trachemys scripta elegans* (*T. scripta*), has been established as a model organism to investigate TSD mechanisms (Fig. 1*A*). *T. scripta* has a warm-female/cool-male TSD system (10). At a constant "warm" incubation temperature of 31 °C (female-promoting temperature, or FPT) during the TSP [Greenbaum stages (St) 15 to 21 (11)], the somatic cells of the bipotential gonad differentiate into granulosa cells and direct ovarian differentiation. Conversely, a continuous "cool" incubation temperature of 26 °C (male-promoting temperature, or MPT) during the TSP causes the somatic cells of the bipotential gonad to differentiate into Sertoli cells, which in turn orchestrate testis differentiation. In *T. scripta*, previous literature showed that some meiotic genes are responsive to retinoic acid (RA) [as in mammals (12, 13)] and are expressed exclusively in FPT gonads around St. 19 (14), demonstrating that the timing of meiotic gene expression is sexually dimorphic at constant warm and cool temperatures. Meiotic progression has not been explored in *T. scripta.* Intriguingly, previous work from our lab showed that warm incubation temperatures directly lead to an increase in germ cell number (15) supporting the hypothesis that temperature directly influences germ cell differentiation. However, whether meiosis is influenced by temperature has not been investigated.

In this study, we show that the transcriptomes of FPT and MPT germ cells are different prior to the differentiation of gonadal somatic cells, consistent with a direct effect of temperature on germ cell differentiation. This result aligns with our previous study, which showed temperature directly influences germ cell number independent of the gonadal soma (15). Here, we demonstrate that although transcription of meiotic genes begins at MPT and FPT, albeit at differing levels, prior to gonad differentiation, prophase I of meiosis begins only in ovaries, after ovarian fate is stabilized. By performing meiotic spreads on germ cells in ovaries developing at MPT, we show that early events of prophase I proceed in accord with the surrounding ovarian soma, however synapsis of homologous chromosomes does not take place. This work demonstrates that germ cell differentiation is impacted by both temperature and the sexual identity of the gonad. These findings suggest that the progression of meiosis to synapsis requires input from both temperature and the somatic gonad.

Results

The Meiotic Transcriptional Program Initiates Asynchronously in FPT and MPT Embryos Prior to Somatic Cell Commitment. To determine when the meiotic transcriptional program is initiated in *T. scripta*, we reanalyzed a single-cell dataset from FPT and MPT embryos at three embryonic stages from the beginning (St. 15), middle (St. 18), and end (St. 23) of the established window of somatic sex determination (Acemel *et al.*, in prep). The recovered 38,063 cells (Fig. 1*B*) were classified into 32 clusters (*SI Appendix*, Fig. S1*A*). Using known marker genes, clusters were assigned to 12 different gonadal cell types that included the germ cells (cell type 8, formed by clusters 19 and 32). This cell type was characterized by high expression levels of *Dazl* (16) and *Ddx4* (*Vasa*) (17) (*SI Appendix*, Fig. S1*B*) and contained cells from all stages and temperature treatments. However, most germ cells belonged to FPT St. 23 gonads (65%, Fig. 1*C*), in line with previous studies demonstrating that higher temperatures result in an increase in the number of germ cells (15). To explore the transcriptional heterogeneity of germ cells, we subclustered them and found 7 subclusters. Subcluster 0 was almost entirely composed of cells from early stages (St. 15 and St. 18) of both MPT and FPT and some late (St. 23) MPT cells. Conversely, the rest of subclusters (1 to 6) were almost exclusively composed of FPT St. 23 cells indicating that transcriptomic changes occur in the germ cells of FPT gonads. To explore these differences, we performed differential expression analysis between subclusters followed by GO enrichments. We found a clear enrichment of terms related to meiosis and cell cycle in clusters 2 to 5 (*SI Appendix*, Fig. S2), suggesting that an asynchronous meiotic onset explains many transcriptomic differences in late FPT germ cells. Of note, we found enrichment in several other processes with known importance in germ cell biology, such as cell migration and extracellular matrix organization.

We then focused on the differential expression of meiotic genes (GO term: *meiotic cell cycle*) classified according to their functions (Fig. 1 *D* and *E* and *SI Appendix*, Fig. S3). Overall, we found that meiotic genes reached their peak of expression in subclusters 2 and 4, with subcluster 4 enriched in replication related genes (*Mcm2*, *Mcm3,* and *Mcm6*). This is also the case with the transcription factors *Mybl1* and *Kctd19*, kinases like the Polo kinase *Plk1*, cyclins like *Ccnb2* and *Ccnb3* or more structural component genes involved in chromosome condensation, synapsis, and spindle assembly (i.e., *Ncapd3*, *Sgo1*, *Cenpe,* or *Sycp2/3*). However, strikingly, transcripts for some meiotic genes like the transcription factor *Stra*8 [considered a master regulator of meiosis (18)], *Msh5* and *Mlh1/3*, which are directly involved in meiotic recombination (19, 20), can be detected in germ cells as early as St. 15 in subcluster 0. St. 15 predates the time when sexual commitment of the somatic cells of the gonad occurs. This observation prompted us to explore whether the early expression of meiotic genes in germ cells was dependent on temperature. To that end, we performed differential expression analysis between FPT and MPT cells restricted to subcluster 0. Interestingly, we found that FPT germ cells were enriched in the GO term "meiotic cell cycle" (*SI Appendix*, Fig. S4) with genes like *Stra8* (18) and *Spo11* (21) being significantly overexpressed when compared to MPT germ cells (Fig. 1 *F* and *G*). Intriguingly, the meiosis negative regulator (22) *Nanos2* was also up-regulated at FPT (*SI Appendix*, Fig. S5*A*), raising the possibility that its expression prevents FPT germ cells from entering meiosis during the TSP. In addition to meiosis, other GO terms were enriched in FPT germ cells like the term "Wnt signaling pathway" (Fig. 1 *H* and *I* and *SI Appendix*, Fig. S5*B*). Intriguingly, among the FPT biased genes, we found several encoding WNT ligands (*Wnt2b* and *Wnt5b*), receptors (*Fzd9*), and both positive (*Sox4* and *Pygo1*) and negative modulators of the pathway (*Dkk1* and *Dact1)*. This pathway has conserved roles in feminizing the somatic gonad and has also been implicated in specification of female germ cells (23, 24). Strikingly, our analyses reveal that MPT and FPT germ cells are already transcriptionally distinct at St. 15, when germ cells have just finished their migration into the undifferentiated gonad (25) and before the gonadal soma has committed to a sexual fate (10). The precocious expression of female-related genes in germ cells prior to somatic differentiation suggests that temperature influences germ cell sexual identity independent of the sex of the gonadal soma.

Cellular Meiotic Onset in Germ Cells Occurs Asynchronously at FPT St. 24, Three Stages After the Completion of Somatic Sex Determination. Our data indicate that transcription of genes associated with meiosis begins in MPT and FPT germ cells by the end of TSP. Next, we set out to define the stage of cellular meiotic onset in *T. scripta* gonads. The first stage of meiosis is prophase I, which is subdivided into five stages—leptotene, zygotene, pachytene, diplotene, and diakinesis. Each stage can be characterized

by chromosome structure and meiosis-specific features (1). In leptotene, meiotic double-strand breaks (DSBs) are initiated and homologous chromosomes pair, typically through the formation of the telomere bouquet, wherein telomeres cluster to one side of the nucleus (Fig. 2*A*). The lateral element (LE) of the synaptonemal complex begins to nucleate at the telomeres. As leptotene transitions into zygotene, the LE nucleates along the chromosome arms. In mid zygotene, the LE is coated along the entire length of the chromosomes, and DSBs persist. At the beginning of pachytene, the LEs from each homologous chromosome are synapsed together along the length of homologs, forming the bona fide tripartite synaptonemal complex, and all DSBs are repaired (26).

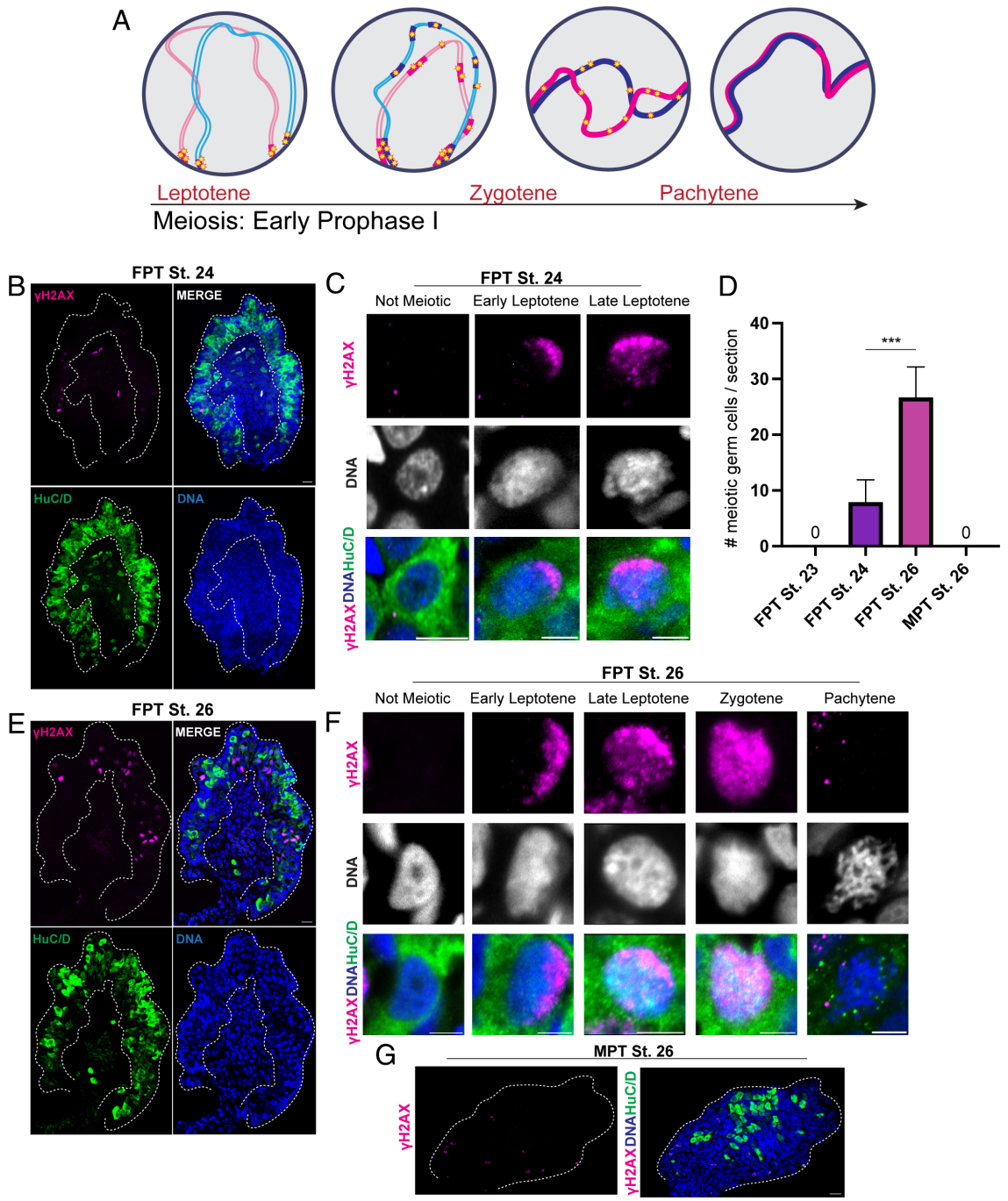

Fig. 2. Cellular meiotic onset occurs at St. 24 in gonads incubated at FPT. (*A*) Generalized early prophase I events. See text for more details. Blue chromosome: replicated sister chromatids; pink chromosome: replicated sister chromatids; blue and pink chromosomes: homologous chromosome pair (2n, 4c). Stars: Meiotic double-strand breaks (DSBs). Thick pink and blue lines represent the synaptonemal complex lateral element protein (SYCP3) on respective homologs. (*B*) Representative image of FPT St. 24 ovary stained with γH2AX (meiotic DSBs, magenta), HuC/D (germ cells, green), and DAPI (DNA, blue). (*C*) Representative images of the three developmental stages of germ cells identified in FPT St. 24 gonads. Stages include "Not Meiotic," "Early Leptotene," and "Late Leptotene." (*D*) Quantification of the number of meiotic germ cells per section, as determined by γH2AX. ***$P < 0.001$, unpaired t test. FPT 23 n = 3 gonads; FPT 24 n = 6 gonads; FPT 26 n = 5 gonads; MPT 26 n = 3 gonads. (*E*) Representative image of FPT St. 26 gonad, stained with γH2AX (magenta), HuC/D (green), and DAPI (blue). (*F*) Representative images of the developmental stages of germ cells identified in FPT St. 26 gonads. Stages shown are "Not Meiotic," "Early Leptotene," and "Late Leptotene," "Zygotene," and "Pachytene." (*G*) St. 26 gonad incubated at MPT. Biological replicates = n > 3 embryos for each experiment. Scale bars *A*, *C*, *E*, 10 μm width, 2 pixels thick. Scale bars *B*, *D*, 5 μm width, 2 pixels thick. Dashed lines in (*B*) and (*E*) outline the ovarian cortex. Dashed lines in (*G*) represent the outline of the testis. All images are of transverse cross sections.

To determine the stage of cellular meiotic onset, MPT and FPT gonads were collected from St. 15 to St. 26, sectioned and stained with HuC/D to identify germ cells (15), γH2AX to determine the presence of DSBs, and DAPI to examine chromatin structure. In FPT gonads, St. 24 was the earliest developmental stage that contained meiotic nuclei (Fig. 2 *B* and *C*), though most germ cells in St. 24 ovaries had not yet entered meiosis ("Not meiotic"), as defined by a lack of γH2AX and a DAPI-negative spherical structure in the nucleus (14). These results indicate that the transcription of meiotic genes precedes the actual cellular onset of meiosis. Meiotic germ cells were staged in early and late leptotene. Early leptotene nuclei exhibited a polar distribution of γH2AX, suggesting the formation of a telomere bouquet, as observed in *Danio rerio* (27), and a distinct absence of the DAPI-negative nuclear structure. Late leptotene germ cells showed a γH2AX signal dispersed throughout the nucleus, though still polarized. At FPT St. 26, the stage just prior to hatching, we observed a significant increase in the number of meiotic germ cells per gonad section as compared to FPT St. 24 (Fig. 2 *D* and *E*, $P < 0.001$), with multiple stages of prophase I represented (Fig. 2*F*). Germ cells in zygotene exhibited a robust, nonpolar γH2AX signal throughout the nucleus. Pachytene germ cells showed highly condensed chromatin and an absence of γH2AX, suggesting complete repair of meiotic DSBs. In contrast to gonads incubated at FPT, we found no meiotic germ cells in MPT St. 26 gonads, as shown by the lack of γH2AX in germ cells (Fig. 2*G*). Together, our results show that, at least under constant incubation conditions, germ cells initiate cellular meiosis asynchronously by St. 24 in ovaries, and just prior to hatching, meiotic germ cells are in various prophase I stages, ranging from leptotene to late pachytene. In contrast, germ cells in MPT testes do not initiate meiosis embryonically.

Synapsis at the Distal Ends of Chromosomes Precedes Synapsis along the Arms. Next, we aimed to determine the relationship between prophase I progression and synaptonemal complex formation within *T. scripta* germ cells. To do this, we examined the localization of the LE protein SYCP3 (28) in various stages of prophase I using chromosome spreads of St. 26 ovaries. Specifically, we examined where SYCP3 initially nucleates on chromosome axes, as represented by stretches of SYCP3 (Fig. 3 *A* and *B*), and we also determined when and where synapsis between homologous chromosomes occurs. Homologous chromosomes were considered

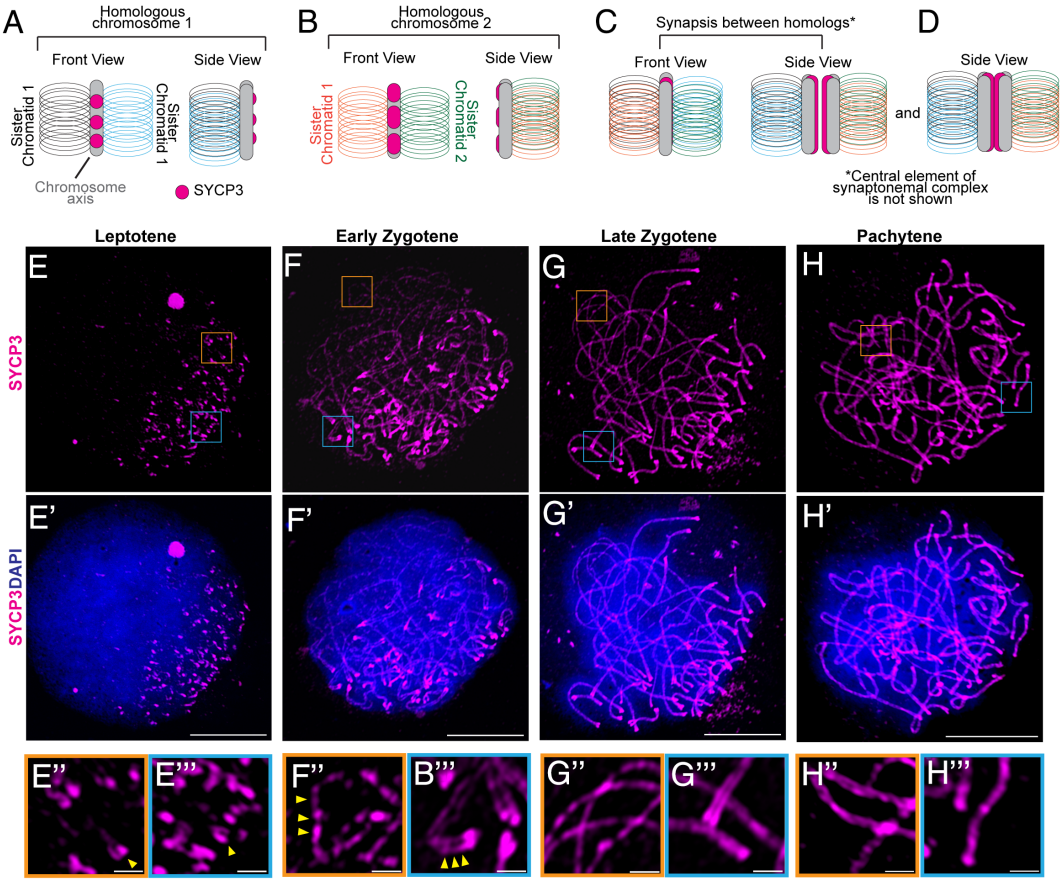

Fig. 3. SYCP3 localization throughout prophase I demonstrates that distal ends of the chromosomes synapse prior to chromosome arm synapsis. (*A*) Schematic of the medial portion (arm) of an unpaired homologous chromosome. The chromosome has two sister chromatids flanking a chromosome axis. Loops represent chromatin. SYCP3 initiates as patches on the axis between the sister chromatids. The front view and side view are shown. SYCP3 is shown as a pink structure. (*B*) Schematic of the chromosome that is homologous to (*A*). (*C*) Front and side view of homologous chromosomes when they are synapsed. SYCP3 is a linear structure and is visualized as two parallel tracks in proximity to each other. (*D*) At this resolution, synapsis of SYCP3 tracts may not be distinguishable. (*E*) Representative image of SYCP3 localization in a leptotene meiotic spread. (*E'*) SYCP3 (magenta) and DAPI (blue). (*E''*) Magnification of orange box in (*E*). The yellow arrow indicates telomere morphology. (*E'''*) Magnification of the blue box in (*E*). The yellow arrow indicates telomere morphology. (*F–F'''*) Representative image of SYCP3 localization in an early zygotene meiotic spread and its respective break-out boxes. *F''* yellow arrows indicate pairing of distal ends of chromosome axes. *F'''* yellow arrows show SYCP3 localization as patches along the chromosome arm. (*G–G'''*) Representative image of SYCP3 localization in a late zygotene meiotic spread and its respective break-out boxes. *G''* and *G'''* show distal and medial areas of chromosomes, respectively. (*H–H'''*) Representative image of SYCP3 localization in a late zygotene meiotic spread and respective break-out boxes. *H''* and *H'''* highlight distal and medial areas of chromosomes, respectively. Scale bars *E'*, *F'*, *G'*, and *H'*, 10 μm. Break-out boxes: 1 μm. Biological replicates = $n > 10$ embryos for each experiment. Contrast and intensity of images in break-out boxes were adjusted uniformly for clarity.

to have experienced synapsis ("synapsed") when two SYCP3 tracks, presumably from homologous chromosomes, are closely associated (Fig. 3 *C* and *D*). From our analysis, a general overview of meiotic progression and synapsis emerged. In leptotene meiocytes, SYCP3 signal was present in short patches (Fig. 3 *E* and *E'*), localizing exclusively at the distal ends of the chromosomes (Fig. 3 *E"* and *E"'*, yellow arrows). The SYCP3 signal at the distal chromosomal ends exhibited extreme polar distribution within the nucleus exclusively at leptotene, which is a well-defined characteristic of the telomere bouquet. In early zygotene, the telomere bouquet was less prominent (Fig. 3 *F* and *F'*). At this stage, homologous telomeres and adjacent distal chromosome regions aligned, as shown by two closely associated tracks of SYCP3 (Fig. 3*F"'*, yellow arrows). However, on chromosome arms, SYCP3 was localized in patches (Fig. 3*F"*, yellow arrows). In late zygotene (Fig. 3 *G* and *G'*), distal ends of the chromosomes were synapsed (Fig. 3*G"*), while chromosome arms were unpaired but exhibited continual stretches of SYCP3 (Fig. 3*G'*). Finally, in pachytene, the telomere bouquet was no longer present (Fig. 3 *H* and *H'*), and full synapsis was achieved, with the SYCP3-containing lateral element of the SC synapsed between homologs at the distal regions of the chromosomes extending throughout the arms. These results align with a previous study that demonstrated that other reptiles, including one with TSD, also form the synaptonemal complex with similar progression (29), wherein the synapsis occurs initially at the telomeres and progresses through the middle of the chromosomes. Additionally, it has been shown that marsupials also exhibit similar meiotic features, including γH2AX polarization (30). Together, our analysis of chromosome spreads demonstrates that the early prophase I events within *T. scripta* are highly conserved and progress similar to other species.

As FPT Germ Cells Enter Meiosis, MPT Germ Cells Continue to Cycle Mitotically. In mammals, germ cells in the ovary differentiate into female gametes by entering meiosis shortly after gonadal sex determination is complete. In contrast, germ cells in the testis differentiate into male gametes by foregoing meiosis and instead entering a long mitotic arrest. Therefore, we sought to determine if, in *T. scripta*, germ cells within the testes enter cell cycle arrest at the same developmental time as ovarian germ cells enter meiosis. To do this, we examined the presence of phospho-H3 (pH3), a marker of meiotic and mitotic metaphase often used to identify mitotically cycling cells (31), in germ cells from St. 24 testes. We observed that approximately 8.46% of germ cells per testis (n = 8 testes, SD ± 2.3 %) were positive for pH3 and exhibited condensed chromatin characteristic of a mitotic nucleus (Fig. 4 *A*–*C*).

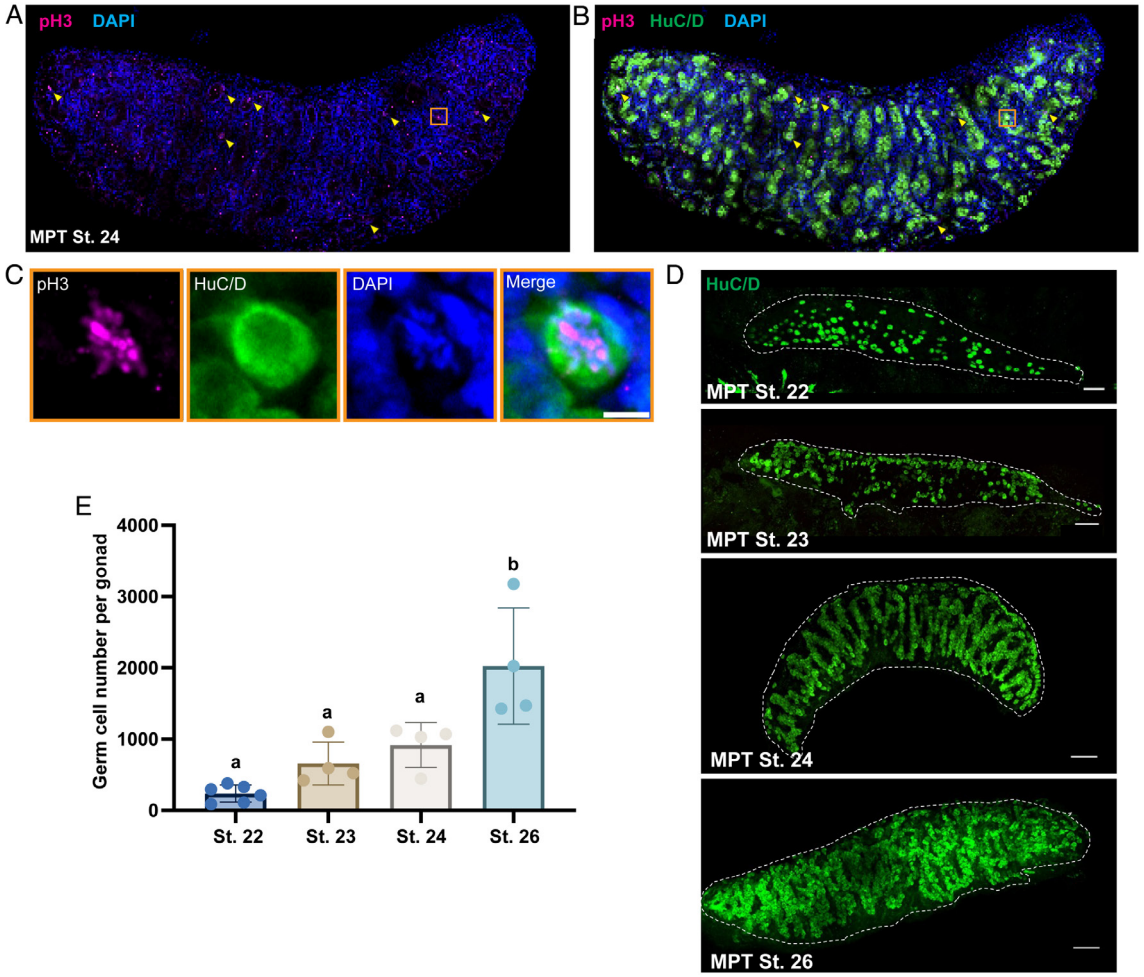

Fig. 4. Germ cells continue to proliferate throughout development at MPT. (*A* and *B*) Representative whole mount image of St. 24 testis. Samples were stained with pH3 (magenta) to label mitotic cells (yellow arrows), HuC/D (green) to label germ cells, and DAPI to label the nuclei. The orange box is magnified in C. (Scale bar, 20 μm.) (*C*) Break-out image of a mitotic germ cell from the testis in *A* and *B*. (Scale bar, 5 μm.) (*D*) Representative images of MPT gonads quantified in (*E*). Samples were stained with HuC/D to identify germ cells. (Scale bar, 100 μm.) (*E*) Quantification of germ cell number per MPT gonads throughout late embryonic development (St. 22 n = 5 gonads, St. 23 n = 4 gonads, St. 24 n = 4 gonads, St. 26 n = 4 gonads). Lowercase letters represent statistically significant groups (a: not significant; b: P = 0.0002; One-way ANOVA). All images are of whole mount testes.

We then reasoned that if germ cells in the testes continued to mitotically cycle throughout embryogenesis, we would observe a steady, linear increase in germ cell number. To test this, we counted germ cells in gonads incubated at MPT from St. 22–St. 26. Despite wide variation among individual samples, we observed a linear increase (R^2 = 0.9804) of germ cells per stage, with means of 236 (±119) germ cells per gonad at St. 22, 659 (±302) at St. 23, and 916 (±316) at St. 24 (Fig. 4 *D* and *E*). At St. 26, we observed a significant increase of germ cells per gonad as compared to stages 22 to 24, with a mean of 2025 (±814) germ cells (P = 0.0002; one-way ANOVA). The R^2 value of germ cell counts from stage 22 to 26 (5 timepoints), with an exclusion of a St. 25 datapoint, was found to be R^2 = 0.9817, indicating germ cell proliferation is linear through the latter end of embryogenesis. The constant rate of proliferation of germ cells between stages suggests there is no drastic change in germ cell cycle progression (*i.e.,* no or few germ cells entering G0) through St. 26. Together, our data demonstrate that while female germ cells enter meiosis asynchronously at the end of embryonic development, male germ cells continue to cycle mitotically until hatching.

Germ Cells in a Feminized MPT Gonad Initiate Meiosis, Yet Exhibit Asynapsis. Previous work from our lab showed that incubation temperature directly influences germ cell number in *T. scripta* prior to the onset of somatic sex determination (15). Additionally, our single-cell RNA-seq results show that FPT germ cells have a distinct transcriptomic profile from MPT germ cells by the beginning of the established TSP. These data led us to question whether it is the incubation temperature (FPT/31 °C or MPT/26 °C), or the sex of the surrounding gonadal somatic cells (granulosa cell in the ovary or Sertoli cells in the testis) that directs the sexual differentiation path of germ cells (*SI Appendix*, Fig. S6*A*). To answer this question, we set out to separate the effects of somatic sex differentiation from incubation temperature by incubating eggs at MPT and treating them with 17β-estradiol (E2) at the beginning of the TSP (St. 15). This is a well-established method that leads to ovary differentiation, despite constant incubation of the gonad at a male promoting temperature (MPT) (32–34). Immunofluorescence analysis of our MPT + E2 treated gonads at St. 26 revealed gonads virtually indistinguishable from control FPT ovaries. These gonads were characterized by an absence of testes cords and the presence of a large cortical domain which housed the germ cells (*SI Appendix*, Fig. S6 *B–D*). These results validate that by adding exogenous E2 to gonads at MPT, we successfully "sex-reversed" the testis to an ovary, thereby separating incubation temperature and gonadal sex. To determine whether germ cells still enter meiosis (*i.e.*, exhibit differentiation into the female gametic fate) in an MPT-incubated but sex-reversed ovary,

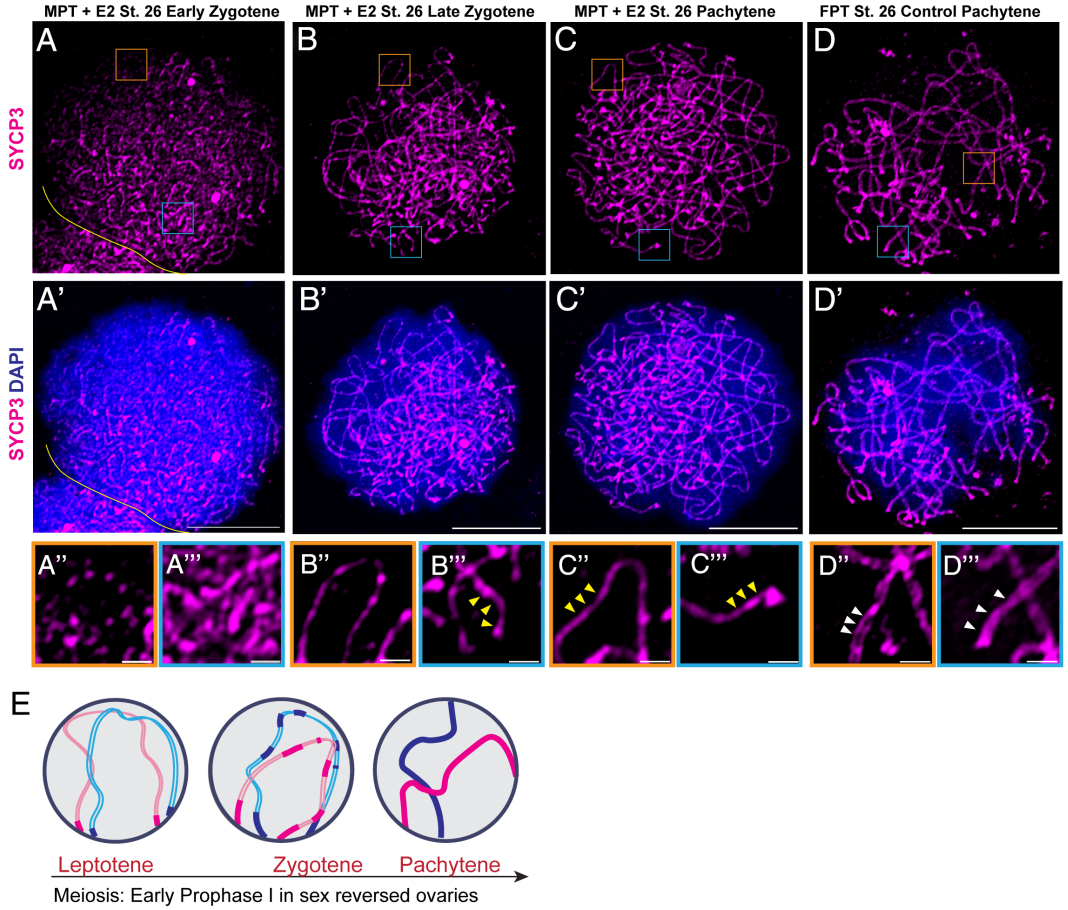

Fig. 5. Meiotic germ cells in MPT+E2 St. 26 spreads build SYCP3 but do not exhibit synapsis at pachytene. (*A*) Representative image of SYCP3 localization in an early zygotene meiotic spread from a sex-reserved ovary. (*A'*) SYCP3 (magenta) and DAPI (blue). (*A''*) Magnification of the orange box in (*A*). (*A'''*) Magnification of blue box in (*A*). (*B–B'''*) Representative image of SYCP3 localization in a late zygotene meiotic spread in MPT + E2 ovary and its respective break-out boxes. *B''* shows SYCP3 localization as patches along the chromosome arm. *B'''* shows lack of synapsis at distal ends of chromosome axes. (*C–C'''*) Representative image of SYCP3 localization in a pachytene meiotic spread in MPT+E2 ovary and its respective break-out boxes. C'' and C''' show medial and distal areas of chromosomes, respectively. (*D–D'''*) Representative image of SYCP3 localization in a germ cell from a St. 26 FPT ovary control at pachytene. *D''* and *D'''* show two tracks of SYCP3, indicating synapsis, which is absent in *C''* and *C'''*. Scale bars *A'*, *B'*, *C'*, and *D'*: 10 μm. Break-out boxes: 1 μm. Biological replicates = n > 10 embryos for each experiment. Contrast and intensity of images in break-out boxes were adjusted for clarity. (*E*) Model of SYCP3 localization but in germ cells from an MPT + E2 sex-reversed ovary.

we examined SYPC3 localization on meiotic spreads of MPT + E2 ovaries at St. 26. We observed germ cells within various stages of meiotic prophase I, with similar timing to control FPT ovaries. The earliest stage identified in MPT + E2 St. 26 samples was early zygotene, wherein the telomere bouquet appeared intact (Fig. 5 *A* and *A*'), and SYCP3 localized in patches on the chromosome arms (Fig. 5*A*"). However, in contrast to germ cells in an FPT gonad at the same stage, we did not observe synapsis at the distal chromosomal ends, as indicated by a lack of parallel SYCP3 tracks (Fig. 5*A*"). In MPT + E2 St. 26 germ cells at late zygotene, SYCP3 nucleation continued along the arms of single chromosomes (Fig. 5 *B*–*B*"), though the distal ends continued to display asynapsis (Fig. 5*B*"', yellow arrows indicate an unsynapsed distal end of a chromosome as compared to Fig. 5*D*"').

Finally, the latest stage we observed in these gonads was a pachytene-like stage (Fig. 5 *C* and *C*'). Here, the telomere bouquet was resolved, and SYCP3 localized as a continuous thread throughout the entire length of the chromosome. However, there was persistent asynapsis, as shown through the single track of SYCP3 on the arms (Fig. 5*C*", yellow arrows), at the distal end of the chromosomes (Fig. 5*C*"', yellow arrows), and the large number of independent chromosome axes in the nucleus. This asynapsis contrasted with a pachytene germ cell from a St. 26 FPT gonad (Figs. 5 *D* and *D*' and 3*H*), which exhibited parallel, closely associated SYCP3 tracks along the entire length of the chromosome arms (Fig. 5*D*", white arrows) to the distal tips (Fig. 5*D*"', white arrows). These data indicate that at least some germ cells from a feminized St. 26 gonad incubated at MPT enter meiosis, and those that do can progress to a pachytene-like stage. However, throughout prophase I progression, the MPT meiotic germ cells exhibit sustained asynapsis.

Discussion

Since the discovery of TSD in 1966 (9), great efforts have been made by the scientific community to understand how temperature influences somatic cell fate decisions in the developing gonad. However, little attention has been placed on the potential influence of incubation temperature on germ cells, even though there is no a priori reason why germ cells cannot also be thermosensitive. Recently, our lab demonstrated that warm incubation temperatures directly influence the number of germ cells during early embryogenesis, prior to the established period of sex determination (15), suggesting that temperature can affect germ cell "behavior" independent of the gonadal soma. Results from the current study also support this hypothesis. First, our single-cell comparative analysis shows that FPT and MPT germ cells have distinct transcriptional landscapes at the beginning of the TSP, prior to the sexual commitment of the gonadal soma between St. 18 to 20. Furthermore, analysis of meiotic spreads on germ cells from 17β-estradiol-feminized MPT gonads demonstrated that when somatic sex does not match the corresponding incubation temperature, germ cells exhibit asynapsis, a meiotic defect that is not present in germ cells from control FPT ovaries. Although ovaries from this well-established treatment (32–34) show no morphological differences as compared to control FPT ovaries, we cannot rule out the possibility that E2 treatment at MPT leads to differences in female soma differentiation that cause downstream effects on meiosis. We plan to investigate this in future experiments via transcriptomic analysis of MPT+E2 gonads. Despite this caveat, our germ cell transcriptome data provide strong supporting evidence that temperature cues influence germ cell sexual differentiation processes independent of the gonadal soma.

Interestingly, our transcriptional and cytological results on FPT germ cells reveal a large temporal gap (7 embryonic stages, equivalent to ~14 d of incubation) between the expression of meiotic genes and the onset of prophase in developing ovaries. Although the reason for this lag between gene expression and actual meiotic entry remains unclear, we speculate that it is related to the long temporal window corresponding to sex determination in *T. scripta*. Depending on incubation temperature, the TSP of sex determination can last anywhere from 12 to 25 d. This represents an ample period where eggs that incubate in the wild might experience an array of temperature cues ranging from MPT to FPT which could result in shifts in gonad trajectory from ovary differentiation to testis differentiation (or vice versa). Under this scenario (which may happen often under natural incubation conditions), we speculate that it would be beneficial for germ cells to "wait" to initiate prophase I until the sex of the gonad is irreversibly committed, ensuring that there is not a mismatch between germ cell differentiation/meiotic progression and the ultimate sexual fate of the gonad. It remains unexplored whether this temporal gap between transcriptional activity and cellular meiotic onset is a conserved phenomenon across species that display TSD or those with a long sex-determining period. How the fate of the soma is coordinated with the germ cells when temperature conditions are fluctuating remains to be established.

While germ cells in FPT ovaries asynchronously entered meiosis soon after sex determination (as in mammals), we observed that germ cells in MPT testes continued to cycle mitotically during the latter end of embryogenesis. In mammals, male germ cell mitotic arrest is a well-conserved phenomenon that is considered essential for normal differentiation of male germ cells into spermatogonial stem cells (35–37). Our findings raise a series of important questions regarding the fate of male germ cell development in *T. scripta.* For example, do male germ cells arrest after hatching? Alternatively, is germ cell arrest dispensable for the establishment of spermatogonial stem cells in certain species? As future studies answer these questions, *T. scripta* could serve as an important comparative model to identify differing mechanisms that drive spermatogonial development.

Importantly, our research provides insights into the factors that influence meiosis in a species with TSD. In our sex-reversed germ cell analysis, we show that female somatic sex is sufficient to initiate germ cell meiotic entry, but in the absence of the correct temperature cue (FPT) during development, germ cells exhibit asynapsis of homologues. Due to antibody limitations in this species, we could not determine whether low incubation temperatures (MPT) affect earlier steps in meiosis, such as double-strand break formation and/or repair. Based on our transcriptome data, we favor the interpretation that warm temperatures directly promote the transcription of gene(s) necessary for normal meiotic progression. Our data suggest that somatic signals from the gonad to the germ cell are not sufficient to ensure sexual differentiation of the germ cell to its oogonial fate. Instead, we propose that two independent cassettes of signals interact to navigate meiosis.

These findings are particularly interesting considering what is observed in many species with GSD. Studies in mice (XX/XY GSD system) have shown that XY germ cells in a sex-reversed XY ovary enter meiosis as in wild-type ovaries. However, germ cell differentiation in these gonads is perturbed (38–40). Further, one study that investigated the precise meiotic defects of sex-reserved ovaries demonstrated that a majority of prophase I germ cells

displayed asynapsis and a reduction in MLH1-specific cross-overs (41). Accordingly, a similar pattern is observed in sex-reversed XX testes, where germ cells enter G0 arrest, as in wild-type testes, yet fail to complete meiosis later in puberty (42). These results are similar to our findings and support a hypothesis that was previously raised (43): that meiotic progression is dependent not only upon the differentiation of the somatic gonad but also upon a matched sexual identity of the germ cell. In species with GSD, this identity is established by sex chromosomes, whereas in TSD species, it is conveyed by the incubation temperature during development. The origin and possible advantages of this dual system remain to be explored.

Materials and Methods

Turtle Eggs. Freshly laid red-eared slider turtle (*Trachemys scripta elegans*) eggs were obtained from Concordia Turtle Farms (Jonesville, LA, with permission from the Louisiana Department of Agriculture). The day after oviposition, fertilized eggs were randomly placed into trays of moist pearlite and housed in incubators kept at either 26 °C (male-producing temperature) or 31 °C (female-producing temperature), with humidity maintained at 70 to 80%. Note that eggs from the same clutches were distributed among the different treatments to minimize clutch bias. Embryos were staged according to criteria established by Greenbaum (11). For all experiments, embryos were removed from eggshells, immediately decapitated, and moved to sterile PBS for gonad dissection.

Male to Female Sex Reversal with 17β-Estradiol. We followed a similar protocol as in ref. 34. Briefly, 5 μl of 17β-estradiol (Sigma, #E8875-1 g) was applied onto the eggshells via micropipette at St. 15. The treatments were applied on the upper portion of the eggshell on the region directly above the vascularized area. Estradiol was dissolved in 95% ethanol at a concentration of 1 μg/μl. Controls received 5 μl of 95% ethanol.

Sc-RNA-seq Analysis. Each single-cell library was aligned to the *Trachemys scripta* assembly and annotation (CAS_Tse_1.0, GCA_013100865.1) using Cell Ranger. The three prime ends of the genes of the annotation were corrected and extended to improve mapping. Quality control of the cells was performed considering the number of reads and features detected, the percentage of mitochondrial transcripts and the contamination with ambient RNA (using DecontX (https://bioconductor.org/packages/decontX/). Doublets were also filtered out using scrublet (https://github.com/swolock/scrublet). The different samples were integrated using SCVI (https://scvi-tools.org/) and SCVI models were also used for differential expression analysis. The number of latent variables was optimized for both the full gonad (latent = 20) and the germ cell subset (latent = 7) by doing a parameter sweep and inspecting the learning curves. Both the UMAP dimensionality reduction and the clusters were calculated from SCVI latent variables using scanpy (https://github.com/scverse/scanpy). Resolutions for Leiden clustering were set at 1.5 for the full gonad and 0.4 for the germ cell subset. Gene Ontology analyses were done using terms associated with mouse orthologs with ClusterProfiler (https://bioconductor.org/packages/clusterProfiler). AUCell (https://bioconductor.org/packages/AUCell/) was used to produce combined scores for the set of genes annotated with *meiotic cell cycle* per cell. The custom R and python code to reproduce the analyses and the figures is available in GitLab (https://gitlab.com/rdacemel/trachemys-meiosis) and contains custom python and R functions gathered in two packages under development, bacarisas (https://gitlab.com/rdacemel/bacarisas, for python) and sorolla (https://gitlab.com/rdacemel/sorolla, for R) which focus in the production of custom plots.

Immunostaining of Whole Mounts and Cryosections. Gonad–mesonephros complexes (GMCs) and whole gonads were dissected in PBS and fixed in 4% PFA for 30 min rocking at room temperature, then moved through a MeOH gradient to 100% MeOH for long-term storage at −20 °C. For immunostaining of whole mounts, after gradual rehydration into PBS, tissues were permeabilized in PBS 0.1 to 1% TritonX-100 for 1 h at room temperature and transferred into blocking solution (PBS 0.1 to 1% TritonX-100, 3% BSA, 10% horse serum) for 2 h. Samples were then incubated with primary antibodies diluted in blocking solution overnight at 4 °C. Following three 30-minute washes in PBS 0.1 to 1% TritonX-100, tissues were incubated with secondary antibodies and DAPI diluted in blocking solution overnight at 4° C. Tissues were then washed three times in PBS 0.1 to 1% TritonX-100 for 1 h at room temperature, mounted for imaging in polyvinyl alcohol-mounting solution and stored at 4 °C until imaged. Note that for gonad samples ranging from St. 15 to 22, the concentration of Triton X-100 was 0.1%, while for samples from St. 22 and above, the concentration was increased to 1%. Samples for cryosection were gradually rehydrated into PBS, moved through a sucrose gradient (10%, 15%, 20%, and 30%), then placed in blocks with OCT medium and moved to −80 °C for a minimum of 12 h before cryosectioning. Blocks were serially sectioned at 12 μm and slides were stored at −20 °C until ready to use. For immunostaining, sections were rehydrated in PBS, permeabilized in PBST (0.1% Triton X-100), and blocked for 1 h at room temperature (PBS 0.1% TritonX-100, 3% BSA, 10% horse serum). Sections were incubated in primary antibodies diluted in Blocking solution at 4 °C overnight. Following three 10-min washes in PBS 0.1% TritonX-100, sections were incubated with secondary antibodies and DAPI diluted in blocking solution for 2 h at room temperature. Following three 10-minute washes in PBST, slides were mounted for imaging with polyvinyl alcohol mounting solution and stored at 4 °C. Whole gonads were imaged using the Andor Dragonfly Spinning Disk confocal microscope and sections were imaged using a 780 Zeiss LSM Confocal Microscope. A series of optical Z sections were collected, and images were analyzed using FIJI (44).

Preparation and Immunostaining of Meiotic Chromosome Spreads. A protocol for *Drosophila* ovarian meiotic spreads (45) was modified and followed. Briefly, prior to dissection, 25 mL of fixative, 5 mL of hypoextraction buffer, and 500 μl of 100 mM sucrose were prepared. Fixative (25 mL): 23.0875 mL water, 1.5625 mL 16% formaldehyde, at 350 μl of 10% Triton-X (1 mL of Triton-X + 9 mL water). Hypoextraction buffer (5 mL): 3.685 mL water, 250 μl 600 mM Tris (pH 8.2), 500 μl 170 mM Trisodium Citrate Dihydrate, 50 μl 500 mM EDTA, 2.5 μl 1.0 M DTT, 12.5 μl 200 mM Pefabloc (hypoextraction buffer is good for only 2 h). 100 mM Sucrose (500 μl): 100 μl 500 mM sucrose + 400 μl water).

Gonads were dissected in 1x PBS and rinsed once in hypoextraction buffer. Gonads were incubated for 30 min in hypoextraction buffer and transferred to sucrose and minced until cloudy. A superfrost slide was dipped into the fixative for 15 s. 10 μl of minced gonads were transferred onto the middle edge of the long side of the slide and rolled to allow spreading. Slides were dried very slowly overnight in a closed humidified chamber. Once dried, slides were incubated with 500 μl of blocking (5% normal horse serum, 2% BSA, 0.1% Triton-X in 1x PBS). Slides were rinsed 3 times in B-PBSTx (0.1% BSA, 0.1% Triton-X in 1x PBS). 250 μl of primary antibodies diluted in B-PBSTx were incubated under parafilm overnight in a humidifying chamber. Slides were washed 3 times with PBSTx (0.1% Triton-X in 1x PBS). Secondary antibodies were diluted at 1:400 in B-PBSTx. 100 μl of diluted secondary were added onto slide under parafilm and incubated for an hour. Slides were rinsed 3 times in PBSTx and washed three times for 10 min in PBSTx in a Coplin jar. Slides were incubated with 400 μl DAPI (1 ug/ml) in 1x PBS for 10 min in dark and washed in 1x PBS. Coverslips were mounted with ProLong Gold. Images were obtained using AIRY-Scan on a Zeiss LSM780 confocal laser scanning microscope using 63x/0.65 NA oil immersion objective. Images were saved as .czi files and processed using FIJI (39).

Statistical Methods. A Mann–Whitney nonparametric *t* test was performed for significance when comparing germ cell numbers between two groups (Fig. 4*E*). A Kruskal–Wallis Test with post hoc Dunn's test with a Bonferroni correction was used to test significance in germ cell counts between multiple stages (Fig. 4*E*). A Fisher exact test was used to assess significance in differences of meiotic germ cells per section (Fig. 2*D*). Data analysis was performed using GraphPad Prism version 10.3.0 for macOS, GraphPad Software, San Diego, California, www.graphpad.com.

Antibody Information

Antibody	Raised in	Concentration	Vendor	Cat. No	Sample Type	Worked? Y/N
γH2AX	Rabbit	1:500	Cell Signaling	9718S	Sections, whole mounts	Y, Y
γH2AX-Alexa Fluor® 594	Rabbit	1:500	Novus Biological	NB100-38AF594	Spreads, sections	N, N
ATM	Rabbit	1:500	Oncogene	PC85	Spreads, sections, whole mounts	N, N, N
CENP-A	Rabbit	1:500	Proteintech	26754	Spreads, sections	N, N
HuC/D	Human	1:50	N/A – Gift from V. Lennon; Mayo Clinic	N/A	Sections, whole mounts	Y, Y
Ki67	Rabbit	1:1,000	Abcam	Ab15580	Whole mounts	N
Ki67	Rabbit	1:500	ThermoScientific	RM-9106	Whole mounts	N
MLH-1	Human	1:500	BD (PharMingen)	554072	Spreads, sections	N, N
MLH-1	Rabbit	1:500	Proteintech	11697	Spreads, sections	N, N
MRE-11	Rabbit	1:500	Proteintech	10744	Spreads, sections,	N, N
pH3	Rabbit	1:500	Cell Signaling	9701S	Whole mounts	Y
SMC3	Rabbit	1:500	Proteintech	14185	Spreads, sections	N, N
SYCE1	Rabbit	1:500	Proteintech	17406	Spreads, sections	N, N
SYCE2 (N-term)	Rabbit	1:500	Abcepta	AP10413a	Spreads, sections, whole mounts	N, N, N
SYCP3	Rabbit	1:500	Abcam	Ab15093	Spreads, sections, whole mounts	N, N, N
SYCP3	Rabbit	1:500	Novus Biological	NB300-231SS	Spreads, sections, whole mounts	Y, N, N
TRF2	Rabbit	1:100	Proteintech	22020	Spreads	N

Data, Materials, and Software Availability. Single cell RNA-seq (scRNA-seq) germ cell data have been deposited in GEO repository (GSE271230) (46). The scRNA-seq germ cell data presented here are derived from a larger dataset from a manuscript that is currently in preparation (Acemel et al., in prep). The larger scRNA-seq dataset will be made publicly available upon deposition of said manuscript in BioRxiv. For thorough review of this study, we provided a private link to a GEO repository where the complete dataset was available to the editor and reviewers.

ACKNOWLEDGMENTS. We thank members of the Capel Lab for thoughtful discussions and feedback. We acknowledge funding from NIH Grant R01HD103064 and NSF Grant 1854642 to B.C. and F32HD113220 to T.H., as well as support from the European Research Council (Grant no. 101045439, 3D-REVOLUTION) and the Spanish "Agencia Estatal de Investigación" (Grant no. PID2022-143253NB-I00/AEI/10.13039/501100011033/ FEDER, UE) to D.G.L. R.D.A. was supported by an EMBO Postdoctoral Fellowship (Grant no. EMBO ALTF 537-2020). Finally, we are grateful to the Duke Light Microscopy Core Facility (NIH Shared Instrumentation Grant 1S10RR027867).

Author affiliations: [a]Department of Cell Biology, Duke University Medical Center, Durham, NC 27701; [b]Biology Department, Wesleyan University, Middletown, CT 06459; [c]Max Delbrück Center for Molecular Medicine in the Helmholtz Association, Berlin Institute for Medical Systems Biology, Epigenetics and Sex Development Group, Berlin 10115, Germany; and [d]Centro Andaluz de Biología del Desarrollo, Consejo Superior de Investigaciones Científicas, Universidad Pablo de Olavide, Junta de Andalucía, Seville 41013, Spain

1. D. Zickler, N. Kleckner, Recombination, pairing, and synapsis of homologs during meiosis. *Cold Spring Harb. Perspect Biol.* **7**, a016626 (2015).
2. P. Berta *et al.*, Genetic evidence equating SRY and the testis-determining factor. *Nature* **348**, 448–450 (1990).
3. P. Koopman, A. Münsterberg, B. Capel, N. Vivian, R. Lovell-Badge, Expression of a candidate sex-determining gene during mouse testis differentiation. *Nature* **348**, 450–452 (1990).
4. B. Capel, Vertebrate sex determination: Evolutionary plasticity of a fundamental switch. *Nat. Rev. Genet.* **18**, 675–689 (2017).
5. A. McLaren, Germ cells and germ cell sex. *Philos Trans. R Soc. Lond. B Biol. Sci.* **350**, 229–233 (1995).
6. A. McLaren, Primordial germ cells in the mouse. *Dev. Biol.* **262**, 1–15 (2003).
7. A. McLaren, The fate of germ cells in the testis of fetal Sex-reversed mice. *J. Reprod. Fertil.* **61**, 461–467 (1981).
8. B. Hilscher *et al.*, Kinetics of gametogenesis. I. Comparative histological and autoradiographic studies of oocytes and transitional prospermatogonia during oogenesis and prespermatogenesis. *Cell Tissue Res.* **154**, 443–470 (1974).
9. N. Valenzuela, V. Lance, *Temperature-Dependent Sex Determination in Vertebrates* (Smithsonian Books Washington, DC, 2004).
10. T. Wibbels, J. Cowan, R. LeBoeuf, Temperature-dependent sex determination in the red-eared slider turtle, Trachemys scripta. *J. Exp. Zool.* **281**, 409–416 (1998).
11. E. Greenbaum, A standardized series of embryonic stages for the emydid turtle Trachemys scripta. *Can. J. Zool.* **80**, 1350–1370 (2002).
12. J. Koubova *et al.*, Retinoic acid activates two pathways required for meiosis in mice. *PLoS Genet.* **10**, e1004541 (2014).
13. J. Bowles *et al.*, Retinoid signaling determines germ cell fate in mice. *Science* **312**, 596–600 (2006).
14. K. Wu *et al.*, Evidence for RA-dependent meiosis onset in a turtle embryo. *Cell Tissue Res.* **394**, 229–241 (2023).
15. B. Tezak *et al.*, Higher temperatures directly increase germ cell number, promoting feminization of red-eared slider turtles. *Curr. Biol.* **33**, 3017–3023.e2 (2023).
16. M. E. Gill, Y. C. Hu, Y. Lin, D. C. Page, Licensing of gametogenesis, dependent on RNA binding protein DAZL, as a gateway to sexual differentiation of fetal germ cells. *Proc. Natl. Acad. Sci. U.S.A.* **108**, 7443–7448 (2011).
17. T. Komiya, K. Itoh, K. Ikenishi, M. Furusawa, Isolation and characterization of a novel gene of the DEAD box protein family which is specifically expressed in germ cells of Xenopus laevis. *Dev. Biol.* **162**, 354–363 (1994).
18. D. B. Menke, J. Koubova, D. C. Page, Sexual differentiation of germ cells in XX mouse gonads occurs in an anterior-to-posterior wave. *Dev. Biol.* **262**, 303–312 (2003).
19. N. M. Hollingsworth, L. Ponte, C. Halsey, MSH5, a novel MutS homolog, facilitates meiotic reciprocal recombination between homologs in Saccharomyces cerevisiae but not mismatch repair. *Genes. Dev.* **9**, 1728–1739 (1995).
20. W. Edelmann *et al.*, Meiotic pachytene arrest in MLH1-deficient mice. *Cell* **85**, 1125–1134 (1996).
21. S. Keeney, C. N. Giroux, N. Kleckner, Meiosis-specific DNA double-strand breaks are catalyzed by Spo11, a member of a widely conserved protein family. *Cell* **88**, 375–384 (1997).
22. A. Suzuki, Y. Saga, Nanos2 suppresses meiosis and promotes male germ cell differentiation. *Genes. Dev.* **22**, 430–435 (2008).
23. A. A. Chassot *et al.*, WNT4 and RSPO1 together are required for cell proliferation in the early mouse gonad. *Development* **139**, 4461–4472 (2012).
24. A. A. Chassot *et al.*, RSPO1/β-catenin signaling pathway regulates oogonia differentiation and entry into meiosis in the mouse fetal ovary. *PLoS One* **6**, e25641 (2011).

25. R. F. Bachvarova, B. I. Crother, A. D. Johnson, Evolution of germ cell development in tetrapods: Comparison of urodeles and amniotes. *Evol. Dev.* **11**, 603–609 (2009).
26. S. L. Page, R. S. Hawley, The genetics and molecular biology of the synaptonemal complex. *Annu. Rev. Cell Dev. Biol.* **20**, 525–558 (2004).
27. Y. P. Blokhina, A. D. Nguyen, B. W. Draper, S. M. Burgess, The telomere bouquet is a hub where meiotic double-strand breaks, synapsis, and stable homolog juxtaposition are coordinated in the zebrafish, Danio rerio. *PLoS Genet.* **15**, e1007730 (2019).
28. M. J. Dobson, R. E. Pearlman, A. Karaiskakis, B. Spyropoulos, P. B. Moens, Synaptonemal complex proteins: Occurrence, epitope mapping and chromosome disjunction. *J. Cell Sci.* **107**, 2749–2760 (1994).
29. L. Marin-Gual *et al.*, Meiotic chromosome dynamics and double strand break formation in reptiles. *Front Cell Dev. Biol.* **10**, 1009776 (2022).
30. F. J. Valero-Regalon *et al.*, Divergent patterns of meiotic double strand breaks and synapsis initiation dynamics suggest an evolutionary shift in the meiosis program between American and Australian marsupials. *Front Cell Dev. Biol.* **11**, 1147610 (2023).
31. M. J. Hendzel *et al.*, Mitosis-specific phosphorylation of histone H3 initiates primarily within pericentromeric heterochromatin during G2 and spreads in an ordered fashion coincident with mitotic chromosome condensation. *Chromosoma* **106**, 348–360 (1997).
32. V. Díaz-Hernández, A. Marmolejo-Valencia, H. Merchant-Larios, Exogenous estradiol alters gonadal growth and timing of temperature sex determination in gonads of sea turtle. *Dev. Biol.* **408**, 79–89 (2015).
33. D. Crews, Temperature-dependent sex determination: The interplay of steroid hormones and temperature. *Zoolog. Sci.* **13**, 1–13 (1996).
34. D. Crews, J. J. Bull, T. Wibbels, Estrogen and sex reversal in turtles: A dose-dependent phenomenon. *Gen. Comp. Endocrinol.* **81**, 357–364 (1991).
35. C. Spiller, D. Wilhelm, P. Koopman, Cell cycle analysis of fetal germ cells during sex differentiation in mice. *Biol. Cell* **101**, 587–598 (2009).
36. G. Du *et al.*, Proper timing of a quiescence period in precursor prospermatogonia is required for stem cell pool establishment in the male germline. *Development* **148**, dev194571 (2021).
37. P. S. Western, D. C. Miles, J. A. van den Bergen, M. Burton, A. H. Sinclair, Dynamic regulation of mitotic arrest in fetal male germ cells. *Stem. Cells* **26**, 339–347 (2008).
38. A. Amleh, L. Smith, H. Chen, T. Taketo, Both nuclear and cytoplasmic components are defective in oocytes of the B6.Y(TIR) sex-reversed female mouse. *Dev. Biol.* **219**, 277–286 (2000).
39. E. H. Park, T. Taketo, Onset and progress of meiotic prophase in the oocytes in the B6.YTIR sex-reversed mouse ovary. *Biol. Reprod.* **69**, 1879–1889 (2003).
40. T. Taketo-Hosotani, Y. Nishioka, C. M. Nagamine, I. Villalpando, H. Merchant-Larios, Development and fertility of ovaries in the B6.YDOM sex-reversed female mouse. *Development* **107**, 95–105 (1989).
41. A. Sakashita *et al.*, XY oocytes of sex-reversed females with a Sry mutation deviate from the normal developmental process beyond the mitotic stage†. *Biol. Reprod.* **100**, 697–710 (2019).
42. M. W. Bradbury, Functional capacity of sex-reversed (XX, Sxr/+) mouse germ cells as shown by progeny derived from XX, Sxr/+ oocytes of a female chimera *J. Exp. Zool.* **226**, 315–320 (1983).
43. J. Bowles, P. Koopman, Retinoic acid, meiosis and germ cell fate in mammals. *Development* **134**, 3401–3411 (2007).
44. J. Schindelin *et al.*, Fiji: An open-source platform for biological-image analysis. *Nature Methods* **9**, 676–682 (2012).
45. T. Hatkevich *et al.*, Centromeric SMC1 promotes centromere clustering and stabilizes meiotic homolog pairing. *PLoS Genet.* **15**, e1008412 (2019).
46. R. D. Acemel *et al.*, Data from "Temperature dependent sex determination in the turtle Trachemys scripta." Gene Expression Omnibus (GEO). https://www.ncbi.nlm.nih.gov/geo/query/acc.cgi?acc=GSE271230. Deposited 1 July 2024.